Preparation of modified montmorillonite/graphene oxide composites to enhance the anticorrosive performance of epoxy coatings

Quanxian Hua, Ben Jing, Mengyuan He, Panfei Sun, Qiang Zhao, Shilong Su, Guanjie Hu, Dehai Ping, Songjie Li

Abstract Modified montmorillonite/graphene oxide composites (AM@GO) were prepared by a hydrothermal method with silane coupling agent-modified montmorillonite (APTES@MMT) and combined with GO. The structures of the composites were characterized by FTIR, XRD, Raman spectroscopy, BET analysis, and SEM. The results showed that the composites had increased interlayer spacing and formed a loosely laminated stacked structure. The specific surface area ($31.6863 \ m^2/g$) and pore volume ($0.0104 \ cm^3/g$) of the composites increased. The hydrophobic and anticorrosive properties of the composite coatings were investigated and compared to the epoxy coating. The composite coatings (AM@GO/EP) had larger contact angles and smoother surfaces than the epoxy coating (EP). After 30 days of immersion, the value of $|Z|_{0.01 \ Hz}$ was approximately $10^{11} \ \Omega \ cm^2$, which had changed slightly since initial immersion. Mechanistic analysis shows that the improved corrosion resistance of the composite coatings was due to the high specific surface area of the 2D material, the oxygen-containing groups of GO, the amino groups of APTES@MMT and the synergy between the MMT and the GO nanosheets.

Keywords Silanized montmorillonite, Graphene oxide, Epoxy coating anticorrosion

Q. Hua, B. Jing, M. He, P. Sun, Q. Zhao,
S. Su, G. Hu, D. Ping, S. Li (✉)
School of Chemical Engineering, Zhengzhou University,
100 Science Avenue, Zhengzhou 450001, People's Republic of China
e-mail: songjie@zzu.edu.cn

Introduction

Epoxy resin coatings, as thermosetting polymers, are commonly used to protect metals from corrosion in corrosive environments due to their low cost, ease of processing, good barrier properties, chemical stability, and high adhesion to metal surfaces. However, when a pure epoxy resin coating is applied directly to metal corrosion protection, its tight three-dimensional network structure is prone to micropores and cracks, leading to brittle fracture of the coating and thus reducing the mechanical properties of the coating.[1,2] The electrolyte makes contact with the metal surface through the cracks in the coating, and the water molecules spread across the metal surface, which destroys the adhesion between the coating and the metal.[3–5] These two factors can significantly reduce the lifetime of the coating. One strategy for overcoming this problem is to modify the coating by adding nanoclay materials to the epoxy resin coating.

Nanoclay has the advantages of a high aspect ratio, large specific surface area, high strength, and high rigidity.[6–8] The addition of nanoclay fillers to the epoxy coating increases the diffusion distance of the electrolyte, and reduces the porosity and the diffusion of ions to the coating/metal interface, thereby reducing the loss of adhesion and improving the mechanical properties of the coating.[9,10] Montmorillonite can be embedded or exfoliated due to its specific layered structure.[11,12] It also has a high cation exchange capacity and a large surface area, which can effectively increase the diffusion distance of the electrolyte in the coating. Due to these factors, nanoclay materials can be used as reinforcing fillers for epoxy resin coating.[6,13] However, the clay flakes are closely attracted to each other due to electrostatic forces and form aggregates in the coating. The aggregates increase the pores and cracks within the film, reducing the mechanical and barrier properties of the coating. Therefore, appropri-

ate surface modification methods must be used to improve the compatibility of montmorillonite with the polymer matrix. Montmorillonite is composed of nanoscale aluminum/silicate sheets in which an alumina sheet is sandwiched between two silicate sheets, resulting in a negative charge.[14] This charge is counteracted by the exchangeable metal ions on the surface of the layer. The exchange capacity of common cations is $Na^+ < K^+ < Mg^{2+} < Ca^{2+} < NH_4^+$, with amino cations having the greatest exchange capacity. Therefore, alkyl organics can be added to promote the insertion or exfoliation of montmorillonite in organic matrices.

In recent years, graphene oxide (GO) has attracted much attention for its easy surface modification, high specific surface area, good acid and base resistance, and high fracture strength.[15–17] It has multiple functional groups and its layered structure is rich in carbonyl, hydroxyl, carboxyl, and epoxy groups.[18,19] The affinity of these functional groups for polar solvents makes it easy to disperse thoroughly into water and other polar solvents by ultrasonication.[20]

These oxygen functional groups can also provide many active sites that facilitate the further modification of GO to tune its properties.[21,22] Hence, the strategy of grafting nanoparticles onto GO has attracted widespread attention. The distribution of GO in the polymer matrix is improved by grafting nanoparticles, and the effective aspect ratio increases.[22,23] It has been reported that vertical van der Waals heterostructure materials with excellent resistance, ideal dielectric properties and atomic plane can be prepared by grafting two-dimensional materials onto GO.[24–26]

To overcome these shortcomings, (3-amino-propyl)-tri-ethoxy-silane (APTES) can be used as a coupling agent to couple GO with nano-montmorillonite. The ANH2 (amine) functional group of APTES can form intercalated structures (AM) with montmorillonite and covalent bonds with GO. In addition, the polar effect of APTES groups helped to improve the dispersion of nanomaterials in epoxy resin coatings.[27,28]

In this work, we investigated the anticorrosion effect of nano-montmorillonite and GO composites in epoxy resin coatings.

The intercalation behavior of the silane coupling agent in montmorillonite and its recombination with GO were analyzed by FTIR, XRD, and Raman spectroscopy. Later, MMT, APTES@MMT, and AM@GO were added to epoxy resin, and their effects on the hydrophobicity and surface roughness of the epoxy coating were investigated by hydrophobic angle and AFM experiments. Finally, their effects on the anticorrosion properties of epoxy coatings were studied by EIS. Figure 1 shows the reaction diagram of the silane coupling agent intercalation modification of montmorillonite and its compounding with GO.

Experimental

Materials

MMT was purchased from Zhejiang Fenghong New Material Co., Ltd, China. APTES (AR) was purchased from Aladdin Reagent (Shanghai) Co., Ltd, China. Graphite powder was purchased from Shanghai Huayi Group Huayuan Chemical Co., Ltd, China. E-44 epoxy resin (EP) and polyamide type curing agent were purchased from Shenzhen Mingde Chemical Co., Ltd, China.

Synthesis of APTES@MMT(AM)

First, 250 mg of MMT was added to the mixed solution of 85 mL of ethanol and 15 mL of distilled water and ultrasonically dispersed for 1 h. Then, APTES was added, and the solution was reacted at 60°C for 7 h. After the reaction, APTES@MMT was obtained by suction filtration, washing, and drying.

Synthesis of GO

One gram of graphite powder (G), and 130 mL of H_2SO_4 and 13 mL of H_3PO_4 were placed in a beaker and stirred for 30 min. Then, 6 g $KMnO_4$ was added to the above mixture very slowly and reacted at room temperature for 2–3 days, turning the solution from black to greenish-brown. H_2O_2 was applied dropwise and the reaction solution turned golden yellow. The reaction sediment was centrifugally washed with 1 moL/L hydrochloric acid and distilled water. The centrifuged product was diluted with water and sonicated for 6 h. The supernatant was dried at 60°C for 6 h to give 0.8 g of brownish red GO.

Synthesis of AM@GO

First, we took two 50 mL beakers, added 30 mL of *N*, *N*-dimethylformamide solution(DMF), respectively, then added 116.7 mg of APTES@MMT and 50 mg GO, respectively, into the above solutions, and performed ultrasonic dispersion for 1 h. Finally, we transferred the solutions in the two beakers to a 100 mL three necked flask, stirred for 30 min, and heated to 130°C to react for 6 h, filtered, cleaned and dried to obtain AM@GO.

Epoxy composite coating preparation

The Q235 carbon steel plates were polished with 100 mesh, 400 mesh, 800 mesh, and 1200 mesh silicon carbide sandpaper, respectively, then put into acetone
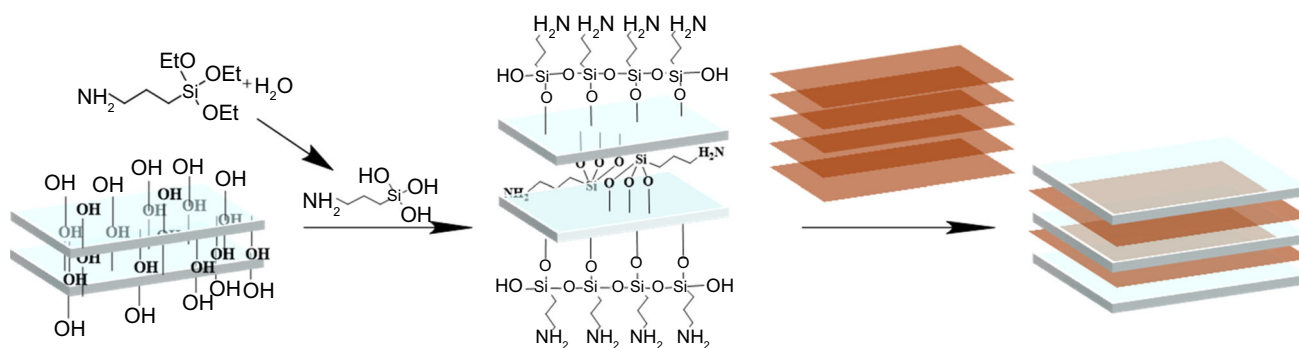
Fig. 1: The reaction mechanism diagram of the combination of GO and APTES@MMT

for ultrasonic cleaning to remove grease and dried for later use.

Firstly, 30 mg of AM@GO powder was added to the xylene/n-butanol mixture (V_{xylene}: $V_{n\text{-butanol}}$ = 7:3) and stirred for 30 min. Then, 7.5 g of E-44 epoxy resin (EP) and 7.5 g of polyamide type curing agent were added, heated, and stirred at 40 °C for 1 h. The filler was mixed well and ultrasonicated for 1 h to remove air bubbles and obtain the AM@GO/EP composite coating. The epoxy composite coating was applied to the surface of the treated steel plate by automatic coating machine (AFA-V, Sichuan Si Chuang Bei Ke technology co., ltd) and adjustable coating machine (BK806, Sichuan Si Chuang Bei Ke Technology Co., Ltd), and cured at room temperature for one week. The average paint film thickness was 100 μm ± 2 μm. The epoxy coating (EP), APTES@MMT/EP, and GO/EP were prepared using the same procedure as described above.

Electrochemical measurements

The electrochemical impedance test used a three-electrode measurement system. The working electrode was a coated steel sheet, the counter electrode was a platinum electrode with a surface area of 2×2 cm^2, and the reference electrode was a calomel electrode. The test electrolyte was a 3.5 wt.% NaCl solution, and the test area was 1 cm^2. The test frequency range was from 10^5 to 10^{-2} Hz, the test temperature was room temperature, and the measurement signal was a sine wave with an amplitude of 10 mV. The test was carried out on PARSTAT MC multichannel multifunctional electrochemical workstation.

Structural characterization

Fourier-transform infrared spectroscopy (FTIR) was performed with a Bruker Tensor-37 spectrometer, and the test wavelength was between 400 and 4000 cm^{-1}. The morphology of the material was observed by high-resolution field emission scanning electron microscopy (SEM, JMS-75000 F). XRD analysis was carried out on a Bruker D8 Advance X-ray diffractometer (Ger-
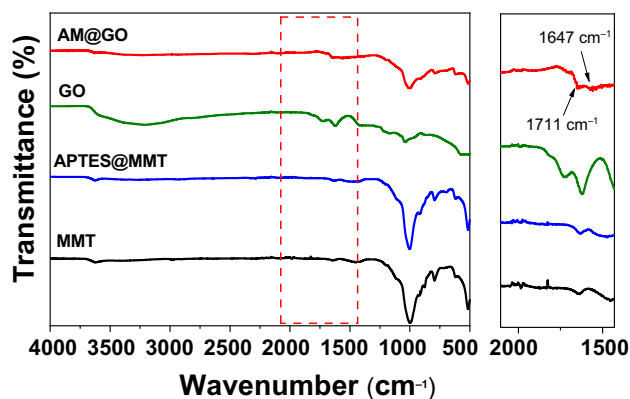

Fig. 2: The FTIR diagram of MMT, APTES@MMT, GO, and AM@GO

many) using CuKα radiation (40 kV, 40 mA and λ = 0.154 nm). Samples were scanned at 2°/min in the range of 2θ = 2–50°. A Horiba Lab RAM HR Evolution Raman spectrometer with a wavelength of 532 nm was used, and the scanning range was from 500 to 3000 cm^{-1}. The BET specific surface area and pore size distribution were calculated on a Micromeritics ASAP-2460 instrument for desorption. The surface roughness of the coating was characterized by a Bruker Dimension Icon atomic mechanics microscope. The hydrophobicity of the coating was analyzed using the Data Physics OCA 20 contact angle tester.

Results and discussion

According to the FTIR spectra of MMT (Fig. 2), strong and broad characteristic absorption peaks were observed at 3625 cm^{-1}, 3400 cm^{-1}, and 3240 cm^{-1}, corresponding to the –OH stretching vibrations of MMT structural water, adsorbed water, and crystal water. The absorption peak at 1436 cm^{-1} can be ascribable to the absorption peak of silicate CO_3^{2-}. The absorption peaks at 1047 cm^{-1} were assigned to the vibration of Si–O–Si skeleton in MMT. The peaks in the range of 800–400 cm^{-1} were attributed to the

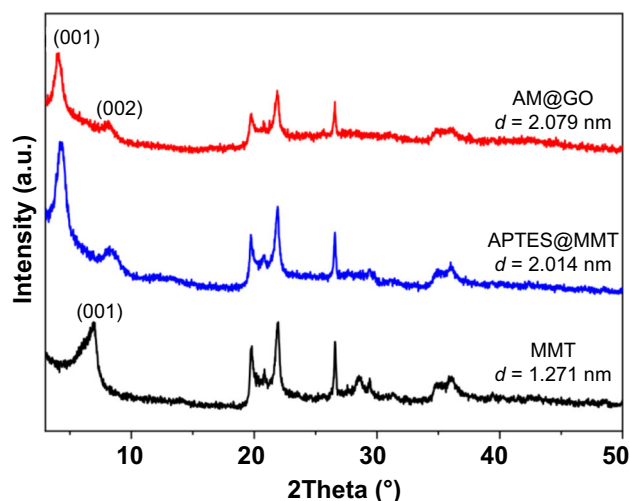Fig. 3: The XRD analysis of MMT, APTES@MMT, and AM@GO

Fig. 4: The Raman analysis of APTES@MMT, GO, and AM@GO

internal vibration of silicon-oxygen tetrahedron and aluminum-oxygen tetrahedron. The appearance of new peaks at 3370 cm^{-1}, 3285 cm^{-1}, and 1483 cm^{-1} was assigned to the stretching and bending vibrations of -NH_2,[29,30] indicating that APTES successfully modified the MMT. The IR spectrum of AM@GO differed slightly from that of APTESS@MMT. A new peak caused by the weak NH bending vibration of the secondary amide bond was observed at 1560 cm^{-1}. Absorption peaks at 1711 cm^{-1} and 1647 cm^{-1} attributed to GO were also observed. The C = O stretching vibration and the C = C conjugate stretching vibration of olefins were partially replaced due to the amide bond, the C = O vibrational peak at 1040 cm^{-1} disappeared and the surface silylated montmorillonite fragments were grafted onto GO.[31]

The XRD pattern in Fig. 3 shows that the (001) peak of MMT shifted significantly, and the peak intensity was constantly variable. The new reflection at approximately 8.5° (2θ) was attributed to the (002) reflection of the silylated product, which was similar to the reflection of the cationic surfactant-modified MMT.[32] After modification by APTES and GO, the d(001) values of MMT, APTES@MMT, and AM@GO were 1.271 nm, 2.014 nm, and 2.079 nm, respectively, indicating that APTES and GO molecules were embedded in the interlayer space of MMT.[33] GO was embedded layer by layer, and the peak intensity was weakened, meaning that the ordered structure of the composite was disrupted and loosely packed together.[34,35] This phenomenon was due to the ring-opening reaction between silane and GO that disrupted the periodic structure of GO and prevented the aggregation of graphene layers.[36]

In the Raman spectra of GO and AM@GO in Fig. 4, the characteristic D-band of the disordered structure (sp^3) at approximately 1350 cm^{-1} and the chara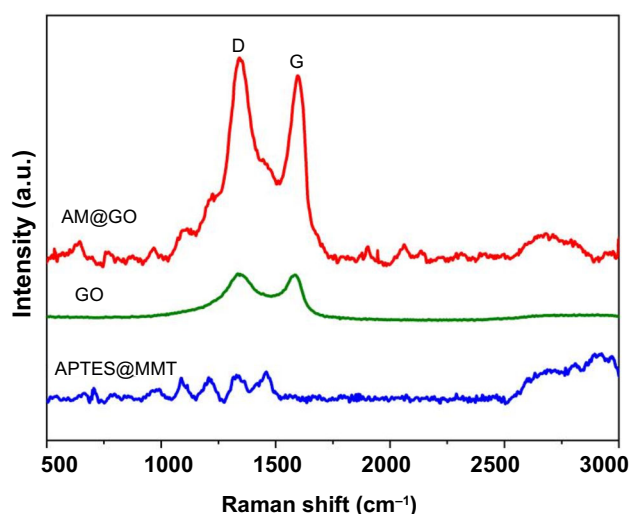cteristic G-band of the ordered structure (sp^2) at approxi-mately 1600 cm^{-1} were observed. The I_D/I_G ratio can be used to estimate the sp^2 domain size and the extent of defects in graphene-based materials. An increase in the ratio indicated that there were more structural defects, more amorphous carbon and a smaller grain size.[37] The strength ratio (I_D/I_G) of GO was 1.021, while the I_D/I_G value of AM@GO increased, indicating that GO and APTES@MMT successfully combined to form a layered stacking structure with increased defects.

Figure 5 shows the N_2 adsorption–desorption iso-therms and pore size distribution curves of AP-TES@MMT, GO, and AM@GO. The hysteresis loop of APTES@MMT exhibited steep adsorption and desorption branches. GO and AM@GO can be cate-gorized as H3 hysteresis loop type II. The specific surface areas of GO and AM@GO were 13.7356 m^2/g and 31.6863 m^2/g, respectively. It can be seen from Fig. 5b that the pore size distributions of MMT, APTES@MMT, GO, and AM@GO were concen-trated, with the pore size distributions of 3.6 nm, 3.63 nm, 3.84 nm, and 3.88 nm, respectively, mainly mesoporous. The surface area and gas adsorption capacity of the AM@GO composites were much higher than those of GO, indicating the presence of a large defect site in the composite and successful material preparation.

Figure 6 shows SEM images of MMT, AP-TES@MMT, GO, and AM@GO. As shown in Fig. 6b, the ordered structure of the MMT flakes was disrupted, and the flakes were stripped and randomly dispersed in the polymer matrix. This result indicated that APTES and MMT compounded successfully. In Fig. 6c, the layered structure of GO was successfully prepared, and GO was partially agglomerated, which may be attrib-uted to strong covalent bonds. In Fig. 6d, the AM/GO composites were uniformly dispersed with reduced agglomeration. Compared to the ordered layered
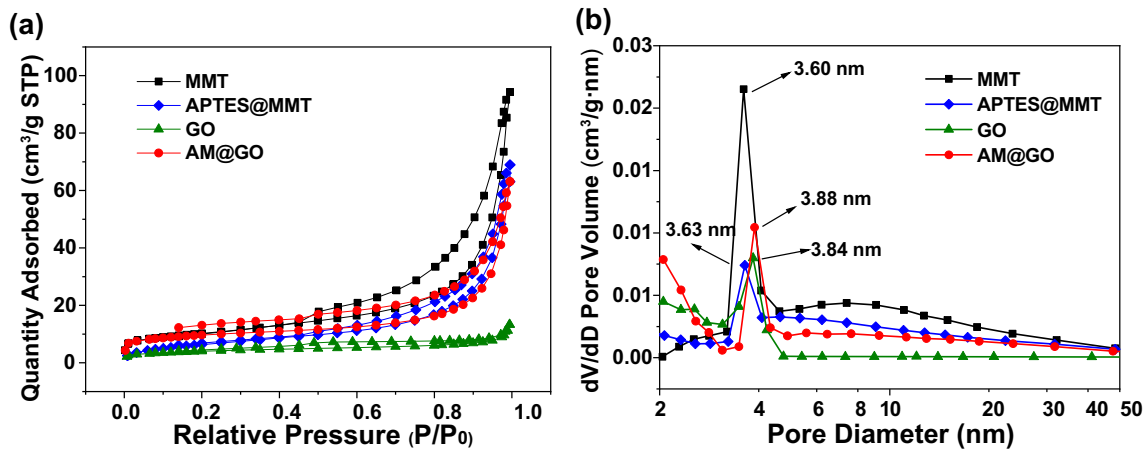
Fig. 5: (a) N$_2$ adsorption–desorption isotherms. (b) Corresponding pore size distribution maps of MMT, APTES@MMT, GO, and AM@GO
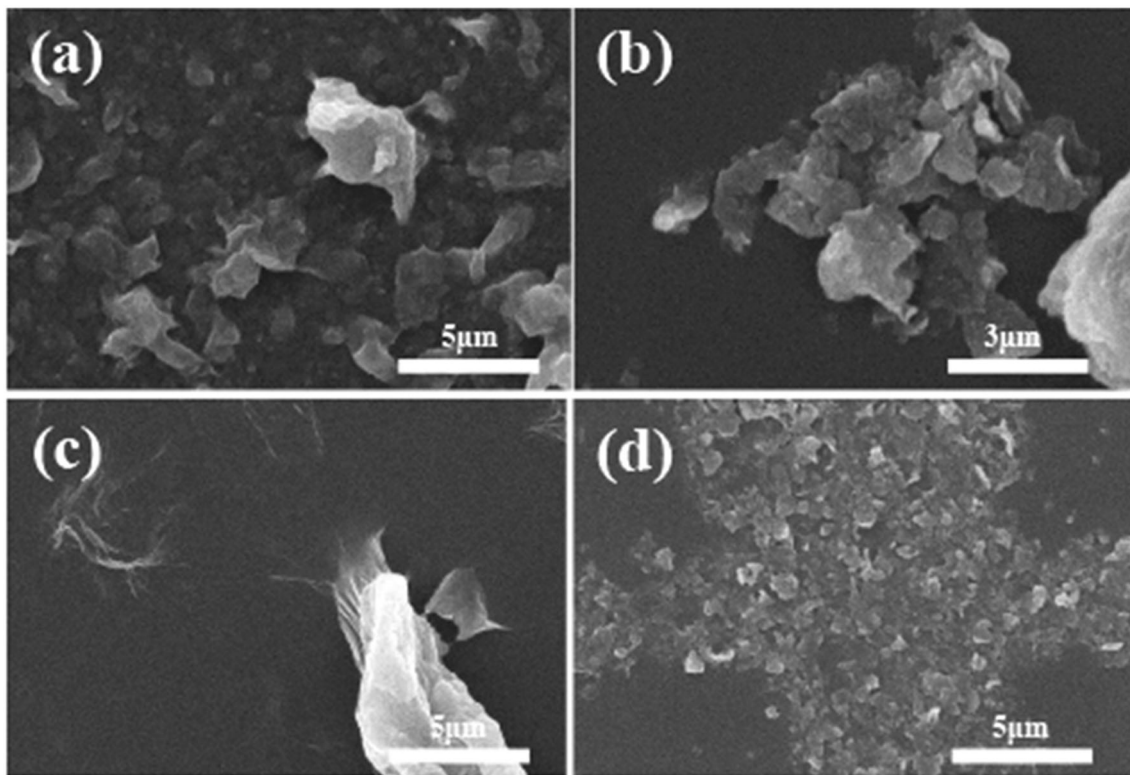

Fig. 6: SEM images of (a) MMT, (b) APTES@MMT, (c) GO, and (d) AM@GO

structure of GO, the composites showed increased layer spacing and looser stacking.

Water contact angle tests on EP, MMT/EP, APTES@MMT/EP, GO/EP, and AM@GO/EP coatings are shown in Fig. 7. With the addition of fillers, the hydrophobicity of the composite coatings was significantly improved. Compared to EP, the composite coatings had increased hydrophobicity due to the hydrophobic functional groups, such as epoxy groups, on the surface of the APTES@MMT, GO, and AM@GO. Of these, the AM@GO/EP coatings exhibit superior hydrophobicity, the hydrophobic angle reached 96°, which was attributed to the increased density of the coating and hydrophobic functional groups of the composites and AM@GO/EP coatings.

The surface roughness of the coatings was tested as shown in Fig. 8. It showed that the surface roughness of EP coating was approximately 45 nm. After adding APTES@MMT, GO, and AM@GO were added, the maximum surface roughness of composite coatings was

7.8 nm and the minimum was 1.6 nm, both smaller than those of the EP coatings. The addition of the composite materials to the EP coating resulted in the smoother coating surface with fewer surface defects. Corresponding to the results of the contact angle test, the lower the surface roughness, the larger the water contact angle.

Figure 9 shows Nyquist and Bode plots of the composite coatings immersed in 3.5 wt.% NaCl aqueous solution for different times. Each Nyquist and Bode plot shows only one time constant, indicating that the coating was effective in protecting the metal in the short term. As can be seen from Table 1, after 30 days of immersion, the impedance modulus of the AM@GO/EP coatings was $10^{10.82}$ Ω cm^2, which is higher than that of other coatings, demonstrating

superior corrosion resistance. This result was attributed to the large number of amino and epoxy groups in the composite, which can be crosslinked with the functional groups in the epoxy resin, creating a two-dimensional material with greatly improved barrier properties. Therefore, the composite materials can be better dispersed in the EP coating, improving the corrosion resistance of the coating.

Conclusions

AM@GO and AM@GO/EP coatings were synthesized by hydrothermal synthesis, and the corrosion resistance of the composite coatings was investigated. XRD proved that APTES intercalation MMT was successful. FTIR, Raman, and SEM proved that AM@GO composite was successfully prepared. The contact angle test proves that AM@GO/EP composite coating has excellent hydrophobicity, and the hydrophobic angle is 96°. AFM proves that AM@GO/EP composite coating has the smallest roughness and the smoothest surface, which corresponds to the contact angle test results. Among the composite coatings, AM@GO/EP had the highest impedance, with a $|Z|_{0.01\ Hz}$ of approximately 10^{11} Ω cm^2 after 30 days of immersion, which was nearly unchanged from the impedance upon initial immersion. The mechanistic analysis suggested that the two-dimensional materials MMT and GO had excellent barrier properties and could effectively enhance the hydrophobic properties of the coating. With the addition of the composite materials to the epoxy coating, the reactive groups on the surface of the materials reacted with the functional groups in the coating, not only increasing the length of the molecular chains but also preventing microscopic cracks from developing. Additionally, the two-dimensional com-
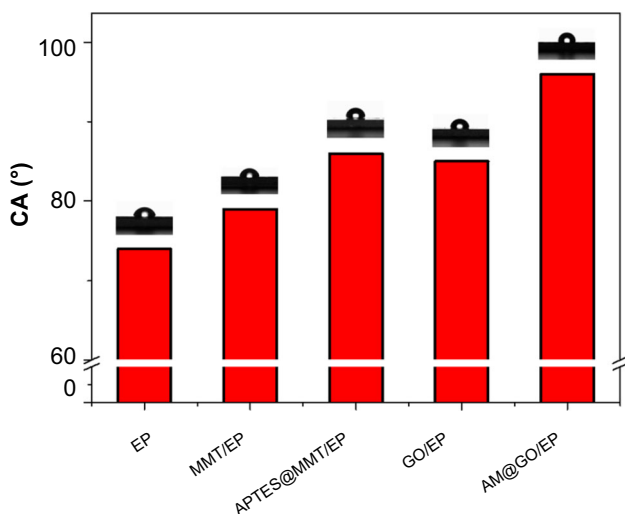

Fig. 7: Test chart of water contact angle of EP, MMT/EP, APTES@MMT/EP, GO/EP, and AM@GO/EP coatings
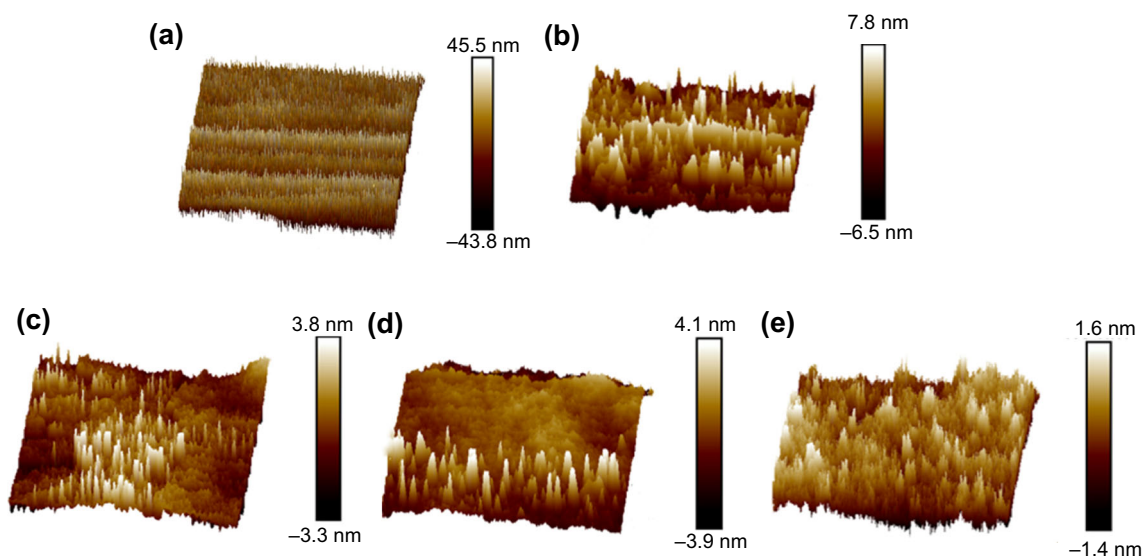

Fig. 8: AFM diagram of (a) EP, (b) MMT/EP, (c) APTES@MMT/EP, (d) GO/EP, and (e) AM@GO/EP coatings

(a)

(b)

(c)

(d)

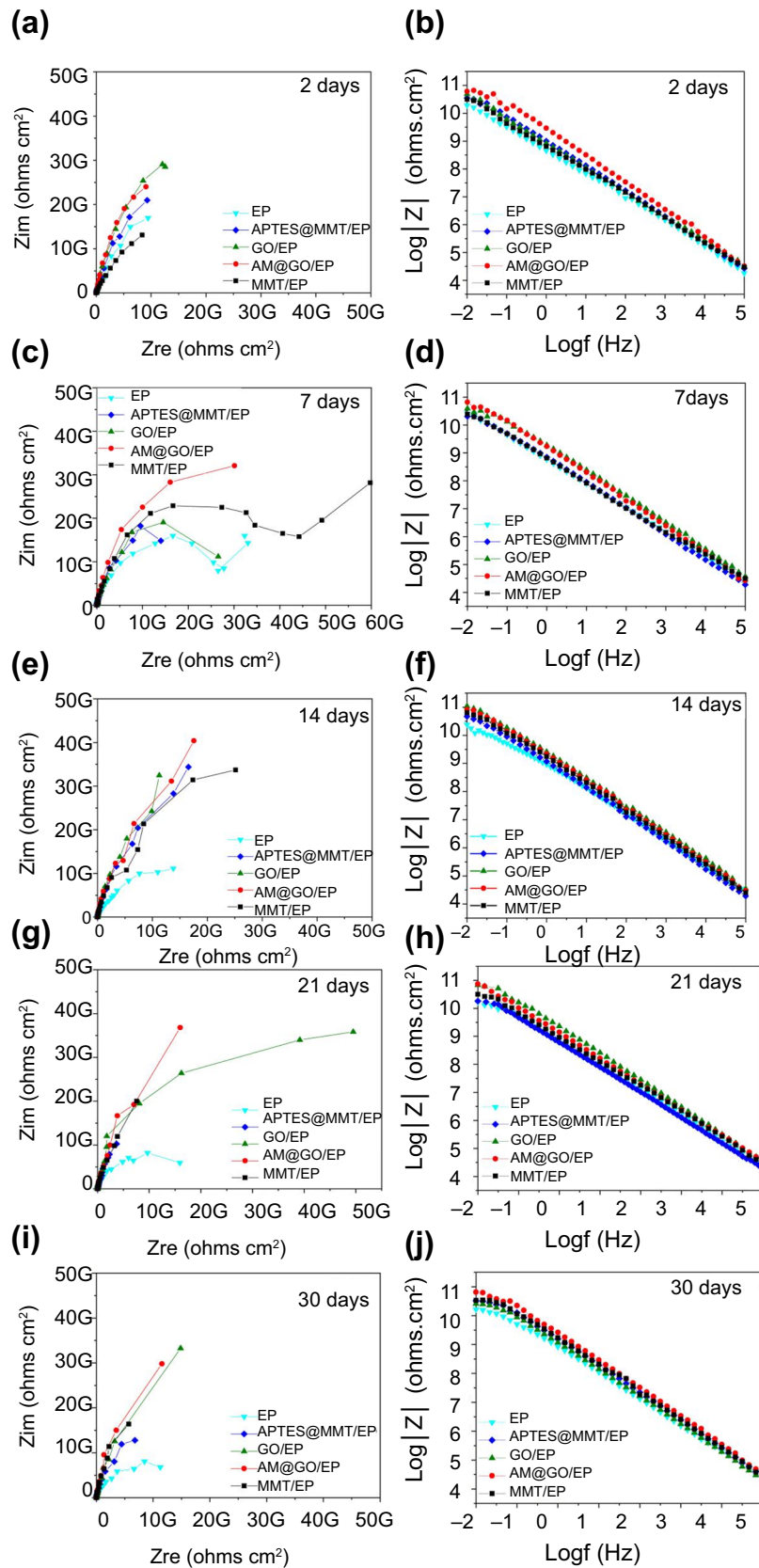**(e)**

(f)

(g)

(h)

(i)

(j)

Fig. 9: (a, c, e, g, i) Nyquist and (b, d, f, h, j) Bode plots immersed in 3.5 wt.% NaCl solution for different times (2d, 7d, 14d, 21d, and 30d) of EP, MMT/EP, APTES@MMT/EP, GO/EP, and AM@GO/EP coatings

Table 1: Impedance values of different types of coatings under different immersion days

Coating type Log|Z| (ohms cm^2) Immersion time (days)	EP	MMT/EP	AM/EP	GO/EP	AM@GO/EP
2	10.29	10.50	10.55	10.69	10.78
7	10.41	10.38	10.31	10.59	10.82
14	10.38	10.80	10.67	11.04	10.91
21	10.23	10.50	10.26	10.83	10.87
30	10.22	10.53	10.52	10.42	10.82

posites formed a large-scale stacked structure, which greatly enhanced the corrosion resistance of the composite coatings. In this study, a new two-dimensional composite was constructed by combining modified MMT with GO to develop a high performance epoxy anticorrosion filler.

Conflict of interest The authors declare that they have no known competing financial interests or personal relationships that could have appeared to influence the work reported in this paper.

References

1. Ji, W-G, Hu, J-M, Zhang, J-Q, Cao, C-N, "Reducing the Water Absorption in Epoxy Coatings by Silane Monomer Incorporation." *Corros. Sci.*, **48** (11) 3731–3739 (2006)
2. Ramezanzadeh, B, Attar, MM, "Studying the Corrosion Resistance and Hydrolytic Degradation of an Epoxy Coating Containing ZnO Nanoparticles." *Mater. Chem. Phys.*, **130** (3) 1208–1219 (2011)
3. Shi, X, Nguyen, TA, Suo, Z, Liu, Y, Avci, R, "Effect of Nanoparticles on the Anticorrosion and Mechanical Properties of Epoxy Coating." *Surf. Coat. Technol.*, **204** (3) 237–245 (2009)
4. Nematollahi, M, Heidarian, M, Peikari, M, Kassiriha, SM, Arianpouya, N, Esmaeilpour, M, "Comparison Between the Effect of Nanoglass Flake and Montmorillonite Organoclay on Corrosion Performance of Epoxy Coating." *Corros. Sci.*, **52** (5) 1809–1817 (2010)
5. Behzadnasab, M, Mirabedini, SM, Kabiri, K, Jamali, S, "Corrosion Performance of Epoxy Coatings Containing Silane Treated ZrO$_2$ Nanoparticles on Mild Steel in 3.5% NaCl Solution." *Corros. Sci.*, **53** (1) 89–98 (2011)
6. Ganjaee Sari, M, Ramezanzadeh, B, Shahbazi, M, Pakdel, AS, "Influence of Nanoclay Particles Modification by Polyester-Amide Hyperbranched Polymer on the Corrosion Protective Performance of the Epoxy Nanocomposite." *Corros. Sci.*, **92** 162–172 (2015)
7. Li, J, Ecco, L, Fedel, M, Ermini, V, Delmas, G, Pan, J, "In-Situ AFM and EIS Study of a Solventborne Alkyd Coating with Nanoclay for Corrosion Protection of Carbon Steel." *Prog. Org. Coat.*, **87** 179–188 (2015)
8. Golgoon, A, Aliofkhazraei, M, Toorani, M, Moradi, MH, Rouhaghdam, AS, "Corrosion and Wear Properties of Nanoclay- polyester Nanocomposite Coatings Fabricated by Electrostatic Method." *Proc. Mater. Sci.*, **11** 536–541 (2015)
9. Navarchian, AH, Joulazadeh, M, Karimi, F, "Investigation of Corrosion Protection Performance of Epoxy Coatings Modified by Polyaniline/Clay Nanocomposites on Steel Surfaces." *Prog. Org. Coat.*, **77** (2) 347–353 (2014)
10. Ghazi, A, Ghasemi, E, Mahdavian, M, Ramezanzadeh, B, Rostami, M, "The Application of Benzimidazole and Zinc Cations Intercalated Sodium Montmorillonite as Smart Ion Exchange Inhibiting Pigments in the Epoxy Ester Coating." *Corros. Sci.*, **94** 207–217 (2015)
11. Soundararajah, QY, Karunaratne, BSB, Rajapakse, RMG, "Montmorillonite Polyaniline Nanocomposites: Preparation, Characterization and Investigation of Mechanical Properties." *Mater. Chem. Phys.*, **113** (2–3) 850–855 (2009)
12. Zhang, Y, Shao, Y, Zhang, T, Meng, G, Wang, F, "High Corrosion Protection of a Polyaniline/Organophilic Montmorillonite Coating for Magnesium Alloys." *Prog. Org. Coat.*, **76** (5) 804–811 (2013)
13. Shirehjini, FT, Danaee, I, Eskandari, H, Zarei, D, "Effect of Nano Clay on Corrosion Protection of Zinc-rich Epoxy Coatings on Steel 37." *J. Mater. Sci. Technol.*, **32** (11) 1152–1160 (2016)
14. Singh-Beemat, J, Iroh, JO, "Characterization of Corrosion Resistant Clay/Epoxy Ester Composite Coatings and Thin Films." *Prog. Org. Coat.*, **74** (1) 173–180 (2012)
15. Du, Y, Li, N, Zhang, T-L, et al. "Reduced Graphene Oxide Coating with Anticorrosion and Electrochemical Property-Enhancing Effects Applied in Hydrogen Storage System." *ACS Appl. Mater. Interfaces*, **9** (34) 28980–28989 (2017)
16. Bai, Y-Y, Wang, F-R, Liu, J-K, "A New Complementary Catalyst and Catalytic Mechanism: Ag$_2$MoO$_4$/Ag/AgBr/GO Heterostructure." *Ind. Eng. Chem. Res.*, **55** (37) 9873–9879 (2016)
17. Hamandi, M, Berhault, G, Guillard, C, Kochkar, H, "Reduced Graphene Oxide/TiO$_2$ Nanotube Composites for Formic Acid Photodegradation." *Appl. Catal. B Environ.*, **209** 203–213 (2017)

18. Novoselov, KS, Geim, AK, Morozov, SV, et al. "Two-Dimensional Gas of Massless Dirac Fermions in Graphene." *Nature*, **438** (7065) 197–200 (2005)

19. Tombros, N, Jozsa, C, Popinciuc, M, Jonkman, HT, van Wees, BJ, "Electronic Spin Transport and Spin Precession in Single Graphene Layers at Room Temperature." *Nature*, **448** (7153) 571–574 (2007)

20. Tong, Y, Bohm, S, Song, M, "The Capability of Graphene on Improving the Electrical Conductivity and Anti-Corrosion Properties of Polyurethane Coatings." *Appl. Surf. Sci.*, **424** 72–81 (2017)

21. Lu, H, Zhang, S, Li, W, Cui, Y, Yang, T, "Synthesis of Graphene Oxide-Based Sulfonated Oligoanilines Coatings for Synergistically Enhanced Corrosion Protection in 3.5% NaCl Solution." *ACS Appl. Mater. Interfaces*, **9** (4) 4034–4043 (2017)

22. Sheng, X, Cai, W, Zhong, L, Xie, D, Zhang, X, "Synthesis of Functionalized Graphene/Polyaniline Nanocomposites with Effective Synergistic Reinforcement on Anticorrosion." *Ind. Eng. Chem. Res.*, **55** (31) 8576–8585 (2016)

23. Yu, Z, Di, H, Ma, Y, et al. "Fabrication of Graphene Oxide–Alumina Hybrids to Reinforce the Anti-Corrosion Performance of Composite Epoxy Coatings." *Appl. Surf. Sci.*, **351** 986–996 (2015)

24. Wahid, MH, Chen, X, Gibson, CT, Raston, CL, "Amphiphilic Graphene Oxide Stabilisation of Hexagonal BN and MoS_2 Sheets." *Chem. Commun.*, **51** (58) 11709–11712 (2015)

25. Sun, G, Bi, J, Wang, W, Zhang, J, "One-Pot Synthesis of Reduced Graphene Oxide@Boron Nitride Nanosheet Hybrids with Enhanced Oxidation-Resistant Properties." *Appl. Surf. Sci.*, **426** 1249–1255 (2017)

26. Liu, Z, Song, L, Zhao, S, et al. "Direct Growth of Graphene/Hexagonal Boron Nitride Stacked Layers." *Nano Lett.*, **11** (5) 2032–2037 (2011)

27. Luo, F, Chen, L, Ning, N, Wang, K, Chen, F, Fu, Q, "Interfacial Enhancement of Maleated Polypropylene/Silica Composites Using Graphene Oxide." *J. Appl. Polym. Sci.*, **125** (S1) E348–E357 (2012)

28. Wang, B, Huang, Y, Liu, L, "Effect of Solvents on Adsorption of Phenolic Resin onto γ-Aminopropyl-triethoxysilane Treated Silica Fiber During Resin Transfer Molding." *J. Mater. Sci.*, **41** (4) 1243–1246 (2006)

29. Huskić, M, Žigon, M, Ivanković, M, "Comparison of the Properties of Clay Polymer Nanocomposites Prepared by Montmorillonite Modified by Silane and by Quaternary Ammonium Salts." *Appl. Clay Sci.*, **85** 109–115 (2013)

30. Chen, W, Zhang, X, Mamadiev, M, Zhao, C, Wang, Z, Xu, H, "Synthesis of Interstratified Graphene/Montmorillonite Composite Material Through Organics-Pillared, Delamination and Co-Stacking and its Application in Hexavalent Chromium Removal from Aqueous Solution." *Adv. Powder Technol.*, **28** (2) 521–533 (2017)

31. Chauhan, DS, Quraishi, MA, Ansari, KR, Saleh, TA, "Graphene and Graphene Oxide As New Class of Materials for Corrosion Control and Protection: Present Status and Future Scenario." *Prog. Org. Coat.*, **147** 105741 (2020)

32. He, H, Frost, RL, Deng, F, Zhu, J, Wen, X, Yuan, P, "Conformation of Surfactant Molecules in the Interlayer of Montmorillonite Studied by ^{13}C MAS NMR." *Clays Clay Miner.*, **52** (3) 350–356 (2004)

33. Zhang, Z, Zhang, J, Liao, L, et al. "Synergistic Effect of Cationic and Anionic Surfactants for the Modification of Ca-montmorillonite." *Mater. Res. Bull.*, **48** (5) 1811–1816 (2013)

34. Wan, Y-J, Tang, L-C, Gong, L-X, et al. "Grafting of Epoxy Chains onto Graphene Oxide for Epoxy Composites with Improved Mechanical and Thermal Properties." *Carbon.*, **69** 467–480 (2014)

35. Ramezanzadeh, B, Haeri, Z, Ramezanzadeh, M, "A Facile Route of Making Silica Nanoparticles-Covered Graphene Oxide Nanohybrids (SiO_2-GO); Fabrication of SiO_2-GO/epoxy Composite Coating with Superior Barrier and Corrosion Protection Performance." *Chem. Eng. J.*, **303** 511–528 (2016)

36. Jiang, T, Kuila, T, Kim, NH, Ku, B-C, Lee, JH, "Enhanced Mechanical Properties of Silanized Silica Nanoparticle Attached Graphene Oxide/Epoxy Composites." *Compos. Sci. Technol.*, **79** 115–125 (2013)

37. Deng, D, Pan, X, Zhang, H, Fu, Q, Tan, D, Bao, X, "Freestanding Graphene by Thermal Splitting of Silicon Carbide Granules." *Adv. Mater.*, **22** (19) 2168–2171 (2010)